

MULTI-TASK TRANSFORMER FOR EXPLAINABLE SPEECH DEEFAKE DETECTION VIA FORMANT MODELING

Viola Negroni*, Luca Cuccovillo†, Paolo Bestagini*, Patrick Aichroth†, Stefano Tubaro*

*Dipartimento di Elettronica, Informazione e Bioingegneria - Politecnico di Milano - Milan, Italy

†Fraunhofer Institute for Digital Media Technology IDMT - Ilmenau, Germany

ABSTRACT

In this work, we introduce a multi-task transformer for speech deepfake detection, capable of predicting formant trajectories and voicing patterns over time, ultimately classifying speech as real or fake, and highlighting whether its decisions rely more on voiced or unvoiced regions. Building on a prior speaker-formant transformer architecture, we streamline the model with an improved input segmentation strategy, redesign the decoding process, and integrate built-in explainability. Compared to the baseline, our model requires fewer parameters, trains faster, and provides better interpretability, without sacrificing prediction performance.

Index Terms— audio forensics, speech deepfake, trustworthy AI, interpretable AI

1. INTRODUCTION

We live in an era of rapid technological change, where AI has quickly become part of everyday life and a driving force across many fields. But this progress also carries serious risks: as society becomes more dependent on AI for routine tasks, and as AI tools become widely available, the chances of malicious use increase, often with harmful consequences.

This problem is especially evident on social media platforms, where the rise of short, easily consumed content makes it easier for people to mistake synthetic media for real information. Among AI-generated media, *deepfakes* refer specifically to synthetic content crafted to mislead or cause harm, and they are increasingly used in fraud, reputational attacks, and to spread misinformation online [1].

Over the years, several data-driven models have been developed specifically for speech deepfake detection, and these detectors have laid a strong foundation in the field [2]. However, the interpretability of these models remains a significant challenge, as it is difficult to determine in advance which speech features are most critical for their predictions of whether a given input is real or fake. Furthermore, neural networks are known to exploit shortcuts during learning [3],

This work was supported by the FOSTERER project, funded by the Italian Ministry of Education, University, and Research within the PRIN 2022 program, and by the news-polygraph project (grant no. 03RU2U151D), funded by the German Federal Ministry of Research, Technology and Space (BMFTR). This work was partially supported by the European Union - Next Generation EU under the Italian National Recovery and Resilience Plan (NRRP), Mission 4, Component 2, Investment 1.3, CUP D43C22003080001, partnership on “Telecommunications of the Future” (PE00000001 - program “RESTART”). This work was partially supported by the European Union - Next Generation EU under the Italian National Recovery and Resilience Plan (NRRP), Mission 4, Component 2, Investment 1.3, CUP D43C22003050001, partnership on “SEcurity and RIghts in the CyberSpace” (PE00000014 - program “FF4ALL-SERICS”).

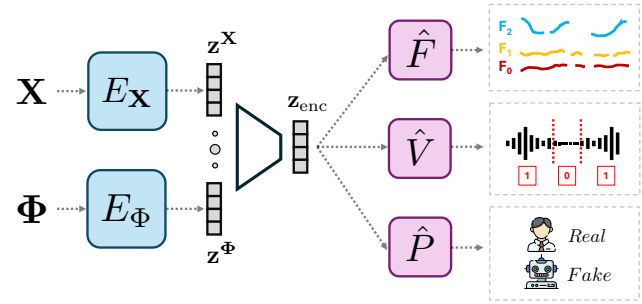


Fig. 1: Illustrative example of the proposed multi-task transformer speech deepfake detector (SFATNet-4).

[4], [5]. Even if this behavior is not inherently problematic, it highlights the importance of understanding what cues a model relies on when making decisions. Indeed, several studies examining detector behavior have shown that many models base their decisions on unvoiced timesteps [6], frequency bands where no speech occurs [7], or even background noise [8], rather than the actual speech. In all these cases, interpretability emerges only *a posteriori*, rather than being embedded in the model design itself.

Newer architectures like SFATNet [9], [10], [11] have been proposed to improve interpretability by design. SFATNet models are hypothesis-driven, meaning their architecture should, in principle, encourage the network to focus on prosodic and speech-related cues. The latest version, SFATNet-3, achieves state-of-the-art performance, matching or surpassing established detectors such as RawNet2 [12] and AASIST [13]. Despite these advances, SFATNet-3 is computationally heavy due to its multi-layer transformer encoder-decoder structure. Moreover, while its outputs are designed to be interpretable, the model still lacks an explicit mechanism for self-explanation.

In this work we introduce SFATNet-4: a new, lightweight speech deepfake detector that is inherently and explicitly interpretable. The proposed system is formulated as a multi-task model, where deepfake detection emerges as a byproduct of auxiliary objectives designed to enhance speech representation and prosodic awareness.

Figure 1 provides an overview of the proposed architecture. A transformer-based encoder, composed of two loosely coupled transformers, processes the magnitude and phase of the input speech signal separately, mapping them into a shared latent representation. On the decoding side, each branch focuses on one task, working at the level of individual time frames. One auxiliary branch encourages the network to learn patterns of prosodic variation by predicting the trajectories of fundamental frequency (F_0) and the first two formants

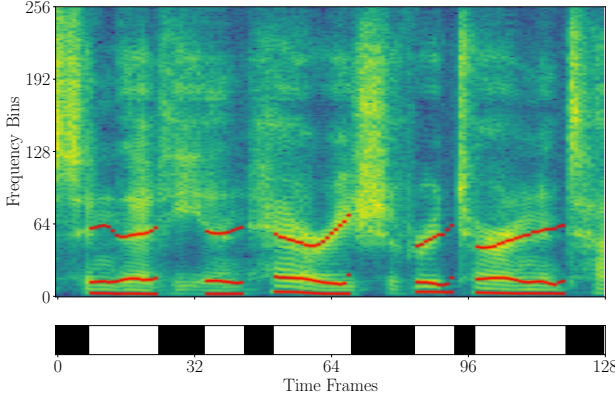


Fig. 2: Example model output for an input spectrogram. Top: original spectrogram with predicted F_0 , F_1 , and F_2 . Bottom: predicted binary voiced/unvoiced segments (voiced: white, unvoiced: black).

(F_1 and F_2) across speech, while another completes this knowledge by learning to distinguish between voiced and unvoiced regions. The third branch focuses on deepfake detection and is equipped with a pooling multi-head mechanism that assigns importance weights to each time frame. These weights not only highlight which segments of speech most influence the final prediction, but also reveal whether the model relied more heavily on voiced or unvoiced regions.

2. PROPOSED SYSTEM

2.1. Problem Formulation

The speech deepfake detection task is defined as follows. Given a discrete speech signal \mathbf{x} with class $y \in \{0, 1\}$ (0: real, 1: fake), the goal is to build a detector $\mathcal{D}(\cdot)$ that outputs $\hat{y} = \mathcal{D}(\mathbf{x}) \in [0, 1]$, the predicted probability of \mathbf{x} being fake.

2.2. Proposed Architecture

The speech deepfake detector $\mathcal{D}(\cdot)$ that we introduce in this work is an enhanced version of the SFATNet-3 model [11], where we aim to improve its efficiency, computational weight, and interpretability. Similar to its predecessor, the new detector is a multi-task audio transformer featuring two encoding modules, one for the magnitude and one for the phase of the input speech signal, and three decoding modules, each dedicated to a distinct task.

The Magnitude Encoder $E_{\mathbf{X}}(\cdot)$ and the Phase Encoder $E_{\Phi}(\cdot)$ are transformer modules built from alternating layers of Multi-Head Self-Attention (MSA) and Multi-Layer Perceptron (MLP) blocks, with layer normalization applied before each block and residual connections applied after, following the standard transformer configuration [14]. On the decoding side, the architecture includes: a Multi-formant Decoder $\hat{F}(\cdot)$ that predicts the evolution in time of the fundamental frequency F_0 and of the two formants F_1 and F_2 , to capture prosodic patterns; a Voicing Decoder $\hat{V}(\cdot)$ that distinguishes between voiced and unvoiced regions; a Synthesis Predictor $\hat{P}(\cdot)$ dedicated to speech deepfake detection.

While $E_{\mathbf{X}}$ and E_{Φ} remain identical to those in SFATNet-3, our model introduces three key changes. First, $\hat{P}(\cdot)$ was modified to enable improved explainability while retaining its original architec-

ture. Second, we completely redesigned $\hat{F}(\cdot)$ to enable more direct and fine-grained formant prediction. Third, we replaced the magnitude reconstruction task of the previous SFATNet versions with the prediction of voiced/unvoiced segments of speech by means of $\hat{V}(\cdot)$. This new task becomes feasible in our architecture thanks to a revised segmentation strategy applied to the input Short-Time Fourier Transform (STFT), a segmentation approach that enables a four-times faster training process. Changes are further detailed in the following.

Speech Preprocessing. Let us denote the short-time Fourier transform of an input sample \mathbf{x}

$$X = \text{STFT}(\mathbf{x}) \in \mathbb{R}^{L \times M}, \quad (1)$$

where L is the number of frames and M the number of frequency bins. From X , we compute the log-magnitude and phase representations as $\mathbf{X} = \log(|X|)$ and $\Phi = \sin(\angle X)$ respectively, maintaining a linear frequency axis. These representations are then segmented to produce input tokens for $E_{\mathbf{X}}(\cdot)$ and $E_{\Phi}(\cdot)$.

In previous work, \mathbf{X} and Φ were segmented to obtain squared patches over both time and frequency as tokens. Our approach segments only along the time axis, producing slices of size $1 \times M$, i.e., a single time frame containing all frequency bins. This time-only segmentation not only reduces complexity and enables efficient processing, but also eventually allows for frame-level interpretability analysis.

Encoding Step. The magnitude and phase tokens are linearly projected to $\mathbb{R}^{L \times D}$ and processed by $E_{\mathbf{X}}$ and E_{Φ} , producing

$$\mathbf{z}^{\mathbf{X}}, \mathbf{z}^{\Phi} \in \mathbb{R}^{L \times D}. \quad (2)$$

These sequences are concatenated (\circ) along the feature dimension D and projected back to the original embedding size by a linear layer:

$$\mathbf{z}_{\text{enc}} \in \mathbb{R}^{L \times D} = \left(\mathbf{z}^{\mathbf{X}} \circ \mathbf{z}^{\Phi} \right) W_{\text{enc}}^{\top} + \mathbf{1}_L \cdot b_{\text{enc}}^{\top}, \quad (3)$$

with $W_{\text{enc}} \in \mathbb{R}^{D \times 2D}$ the projection matrix, $b_{\text{enc}} \in \mathbb{R}^{D \times 1}$ the bias vector, and $\mathbf{1}_L \in \mathbb{R}^{L \times 1}$ a L -dimensional column vector of ones.

Multi-formant Decoder $\hat{F}(\cdot)$. Formants are the resonant frequencies of the vocal tract that shape the sound of speech. They are influenced by the positioning and shape of the throat, mouth, and nasal passages as air flows through them. In SFATNet-3, the three primary formants (F_0 , F_1 , F_2) were predicted via a transformer module producing a matrix-like representation.

In contrast, our model directly predicts the continuous trajectory of each formant, estimating its value for every input frame. A linear projection maps the encoded tokens \mathbf{z}_{enc} to a sequence $\mathbf{z}^{\hat{F}}$ of three values per frame. These values are then converted to the final output \hat{F} , representing the predicted formant trajectories across all L frames by means of

$$\hat{F} \in \mathbb{R}^{L \times 3} = \left\{ \left(\sigma(\mathbf{z}_i^{\hat{F}}) \cdot F_i^+ + F_i^- \right) \right\}_{i \in \{1, 2, 3\}}, \quad (4)$$

with $\sigma(\cdot)$ the sigmoid function, and F_i^+ , F_i^- the upper and lower limit of the i -th formant. The ranges were selected according to physiologically plausible ranges, resulting in $F_0 \in [60, 400]$ Hz, $F_1 \in [200, 850]$ Hz, and $F_2 \in [800, 2700]$ Hz.

This design removes the need for an additional transformer decoder for formants, and produces more interpretable frame-level predictions. The top part of Figure 2 illustrates the reconstructed formants of an example track on the original spectrogram, highlighting how the model effectively captures the speech structure.

Voicing Decoder $\hat{V}(\cdot)$. This module replaces the magnitude reconstruction task in previous SFATNet versions by predicting voiced and unvoiced frames from the encoding embeddings \mathbf{z}_{enc} . Voiced frames are the ones in which vocal folds vibrate during speech production, whereas unvoiced frames correspond to sounds without vocal fold vibration and to non-speech segments. A linear projection to $\mathbb{R}^{L \times 1}$ with sigmoid activation produces a probability for each frame, where frames with probability ≥ 0.5 are classified as voiced, as in the bottom part of Figure 2, where the predictions of $\hat{V}(\cdot)$ over the example track are reported visually. Importantly, the resulting binary mask $v_{\text{mask}} \in \{0, 1\}^{L \times 1}$ is used to avoid formant prediction for unvoiced segments by refining the output of $\hat{F}(\cdot)$.

Synthesis Predictor $\hat{P}(\cdot)$. This module consists of a sequence-to-sequence transformer the output of which is pooled over time with a multi-head mechanism [15], [16], where tokens are scored via $\log\text{-sumexp}$ and softmax to produce frame-level weights.

Let us denote with $\mathbf{z}^{\hat{P}} \in \mathbb{R}^{L \times D}$ the raw output sequence of the transformer, given the input sequence \mathbf{z}_{enc} . This raw output can be pooled by means of:

$$\mathbf{z}_{\text{pooled}}^{\hat{P}} \in \mathbb{R}^{1 \times D} = \text{softmax} \left(\log(\exp(\mathbf{z}^{\hat{P}} \cdot W_H) \cdot \mathbf{1}_H) \right)^{\top} \cdot \mathbf{z}^{\hat{P}}, \quad (5)$$

with $W_H \in \mathbb{R}^{D \times H}$ the learned projection matrix for H attention heads. The pooled embedding can finally be converted into the synthesis prediction score \hat{y} through layer normalization and a linear projection.

By replacing the standard class-token of earlier SFATNet versions with a pooling step, $\hat{P}(\cdot)$ is aligned with the other frame-level decoding modules, as it allows us to obtain one weight w_l for each output element of the softmax layer, i.e., one attention score for each frame in the input sequence. The pooling weights thus also reveal which frames drive the decision, enabling frame-level explainability that can be paired with the voicing predictor to assess whether the model relies more on voiced or unvoiced regions of speech.

3. EXPERIMENTAL SETUP

3.1. Datasets

We consider 4 speech deepfake datasets to assess both in-domain performance and out-of-domain generalization. All speech is resampled to 16 kHz for consistency across datasets.

- **ASVspoof 5** [17]. Released for the 2024 edition of the homonymous challenge, this dataset was created through a crowdsourcing process, collecting data across a wide variety of acoustic environments. It features fake speech from 32 generators, a combination of both legacy and state-of-the-art Text to Speech (TTS) and Voice Conversion (VC) models.
- **In-the-Wild** [18]. This dataset is designed to evaluate speech deepfake detectors in realistic scenarios. Audio clips from 54 celebrities and politicians were obtained by segmenting publicly accessible video and audio content.
- **FakeOrReal** [19]. This dataset consists of both synthetic and real speech samples. Fake samples were generated using 7 different open-source and commercial TTS systems. Real speech samples were sourced from publicly available platforms.
- **TIMIT-TTS** [20] A dataset of fake audio samples, generated from 12 different TTS methods. We paired it with its real counterpart, VidTIMIT [21], and consider its *clean* partition.

We train our model on ASVspoof 5 without any data augmentation, merging the *train* and *dev* partitions, splitting the resulting data 90/10, and oversampling real speech to maintain balanced classes. In-domain testing is performed on ASVspoof 5 *eval* partition. We also assess the model intrinsic generalization by evaluating it on three unseen datasets: In-the-Wild, FakeOrReal, and TIMIT-TTS.

3.2. Training Specifications

The ground truth annotations for F_0 were extracted using the pYin algorithm [22], a probabilistic pitch tracker that robustly estimates fundamental frequency trajectories. Since F_0 is only defined in voiced regions, frames where pYin yields a valid F_0 correspond to voiced segments, while frames without a pitch estimate can be classified as unvoiced. Hence, these F_0 annotations also provide supervision for the voicing decoder $\hat{V}(\cdot)$. This dual role ensures consistency across decoders: the Multi-formant Decoder $\hat{F}(\cdot)$ is supervised by continuous F_0 contours, while the Voicing Decoder $\hat{V}(\cdot)$ is trained with a binary voicing mask derived directly from the same ground truth signal, preventing contradictory predictions such as unvoiced decisions in regions with nonzero pitch.

Higher-order formants (F_1, F_2) were obtained using Parselmouth’s Burg formant tracker [23], [24]. The frame and hop length we used are 0.032 s and 0.016 s, respectively. These values were also used for the STFT in the model’s preprocessing step, yielding $M = 256$ frequency bins and $L = 128$ time frames. In other words, the system processes fixed-length inputs of 2.064 s, corresponding to 33.024 samples. Shorter inputs were padded by repeating the signal, while longer utterances were truncated to match the required length. We removed leading and trailing silence and normalized the audio so that peak amplitudes reach 1.0, to eliminate common shortcut artifacts that neural networks might otherwise exploit [17].

As in SFATNet-3, the magnitude and phase encoders $E_X(\cdot)$ and $E_{\Phi}(\cdot)$ consist of 8 transformer layers, with MSA modules of 8 heads (dimension 64) and MLP blocks in 1024 dimensions. The synthesis predictor $\hat{P}(\cdot)$ also retains the same layout: 4 transformer layers, MSA with 6 heads (dimension 64), and MLP blocks in 1024 dimensions. The embedding dimension is $D = 512$ for all modules. The new multi-head weighting mechanism in $\hat{P}(\cdot)$ has $H = 4$ heads.

The training used a batch size of 256 with the AdamW optimizer and an initial learning rate of 10^{-4} , which decays after 10 epochs of plateau. In contrast to SFATNet-3, no masking was applied to the encoders during training. The model was trained for 100 epochs with early stopping (patience 20), monitoring the validation loss. The compound loss combined a Binary Cross Entropy (BCE) loss for \hat{P} , a BCE loss for \hat{V} , and a Mean Squared Error (MSE) loss for \hat{F} , with weights 1, 0.3, and 0.3, respectively. To stabilize training, both target and ground-truth formants were first log-scaled and then standardized using means and standard deviations computed from the training set. During the MSE loss computation, only voiced frames are used to penalize the model. On an NVIDIA A40 GPU, the model requires approximately 15 min to train a single epoch, compared to over 60 min for SFATNet-3. The number of parameters was reduced from 64.7M to 41.8M.

4. RESULTS

4.1. Performance and generalization

In Table 1, we compare the performance of our proposed model with its predecessor, SFATNet-3. In-domain performance is evaluated on

Table 1: Comparison of EER (%) and AUC (%) across datasets for the proposed model and SFAT-Net 3.

	ASVspoof 5		In-the-Wild		FakeOrReal		TIMIT-TTS		Average	
	EER ↓	AUC ↑	EER ↓	AUC ↑	EER ↓	AUC ↑	EER ↓	AUC ↑	EER ↓	AUC ↑
Proposed	4.41	98.89	17.29	89.17	20.33	85.03	20.93	84.49	15.74	89.40
SFAT-Net 3	8.85	96.69	19.70	85.20	21.08	81.01	18.59	83.36	17.06	86.57

Table 2: Robustness of the proposed model across ASVspoof 5 codecs. Best in **bold**, worst in *italic*.

	Codec	MP3	M4A	Opus	AMR	Speex
EER (%)	29.2	<i>40.9</i>	21.8	28.2	34.2	32.0
AUC (%)	77.5	64.9	85.6	79.3	71.6	74.7

ASVspoof 5 (clean subset, no codecs), out-of-domain generalization is tested on In-the-Wild, FakeOrReal, and TIMIT-TTS. Results are reported in terms of Equal Error Rate (EER) and Area Under the Curve (AUC). Both models excel on the in-domain benchmark, with AUC values above 95%. Performance drops out-of-domain due to distribution shifts, as expected from omitting data augmentation, though both models remain reasonably robust. Our proposed model outperforms SFATNet-3 on nearly all datasets, achieving lower EER and higher AUC. These results confirm the superiority of the proposed architecture both on seen data and unseen conditions.

4.2. Robustness by design

Robustness to common compression standards is essential for reliable deployment of spoofing detectors. In Table 2, we assess the intrinsic robustness (without training data augmentation) of our architecture by testing on codec-processed data from ASVspoof 5. Results are broken down by codec type. Compared to in-domain results on clean data (Table 1), performances drop across all compression systems, the largest degradation being with MP3, and M4A showing higher resilience. When narrow-band (8kHz) data, available for Opus, AMR, and Speex, are considered performance drops further by 16.8%, 12.0%, and 14.7% AUC, respectively. Notably, the model maintains solid discriminative power under the newer neural codec Encodec. Therefore, our model shows some inherent robustness, but data augmentation is required for reliable real-world performance.

4.3. Explainability analysis

The new input segmentation by time frames, combined with the pooling attention mechanism introduced in $\hat{P}(\cdot)$, enables *temporal explainability* by highlighting the frames that contribute most to the model decisions. When paired with the voicing predictor, also producing frame-level outputs, this makes it possible to determine whether the model relies more on voiced or unvoiced regions of speech for its predictions. For this analysis, we focus on correctly predicted samples using the threshold corresponding to the model EER, and we compute averages over all frame-level scores weighted by their attention values. Since the attention weights are very sparse in our case, this approach produces results that are essentially equivalent to a top-k study. Figure 3 presents the analysis of our model for the outcomes in Table 1.

For in-domain data from ASVspoof 5, the model shows a nearly equal reliance on voiced and unvoiced regions when processing real

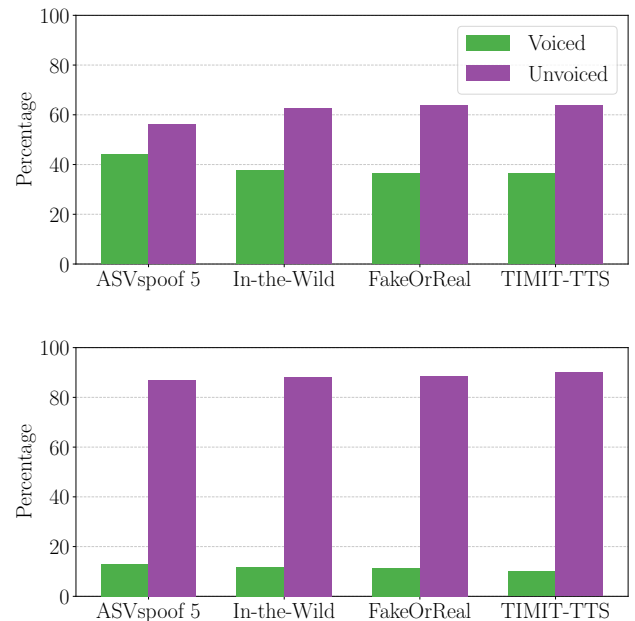


Fig. 3: Relative importance of voiced and unvoiced frames for correctly classified speech. Each pair of bars shows the contributions of voiced and unvoiced frames to the model’s decision in a specific dataset, as weighted by the model’s attention scores. Top: real speech; bottom: fake.

speech. For out-of-domain data, however, the model draws more cues from unvoiced parts of speech, which may correspond to speech segments without formants or to non-speech regions. Interestingly enough, for synthetic speech, the model consistently relies heavily on unvoiced regions. This suggests that the most salient synthesis artifacts are found in unvoiced segments, an observation that aligns with previous studies [6].

5. CONCLUSIONS

In this work we presented SFATNet-4: a novel, lightweight multi-task transformer for speech deepfake detection. The model, designed for interpretability, simultaneously captures prosodic patterns, distinguishes voiced from unvoiced segments, and identifies manipulated speech. The integration of attention-based mechanisms and auxiliary tasks not only enhances detection performance but also provides insight into the cues driving the model’s decisions, addressing a critical gap in current approaches. Our results show that interpretability may be improved without sacrificing performance, paving the way for more transparent and accountable speech deepfake detection systems. Future work will extend SFATNet-4 to multilingual speech, expand prosodic features, and optimize it for real-time use.

6. REFERENCES

- [1] I. Amerini et al., “Deepfake media forensics: Status and future challenges,” *MDPI Journal of Imaging*, vol. 11, no. 3, p. 73, 2025.
- [2] M. Li, Y. Ahmadiadli, and X.-P. Zhang, “A survey on speech deepfake detection,” *ACM Computing Surveys*, vol. 57, no. 7, 2025.
- [3] R. Geirhos et al., “Shortcut learning in deep neural networks,” *Nature Machine Intelligence*, vol. 2, no. 11, pp. 665–673, 2020.
- [4] N. M. Müller, F. Dieckmann, P. Czempin, R. Canals, K. Böttiger, and J. Williams, “Speech is silver, silence is golden: What do asvspoof-trained models really learn?” In *ASVspoof Challenge Workshop*, Brno, Czech Republic, 2021.
- [5] V. Negroni, D. Salvi, P. Bestagini, and S. Tubaro, “Analyzing the impact of splicing artifacts in partially fake speech signals,” in *ASVspoof Challenge Workshop*, Kos Island, Greece, 2024.
- [6] G. Sivaraman, H. Tak, and E. Khoury, “Investigating voiced and unvoiced regions of speech for audio deepfake detection,” in *IEEE International Conference on Acoustics, Speech and Signal Processing (ICASSP)*, Hyderabad, India, 2025.
- [7] D. Salvi, P. Bestagini, and S. Tubaro, “Towards frequency band explainability in synthetic speech detection,” in *European Signal Processing Conference (EUSIPCO)*, Helsinki, Finland, 2023.
- [8] D. Salvi, T. S. Balcha, P. Bestagini, and S. Tubaro, “Listening between the lines: Synthetic speech detection disregarding verbal content,” in *IEEE International Conference on Acoustics, Speech, and Signal Processing Workshops (ICASSPW)*, Seoul, South Korea, 2024.
- [9] L. Cuccovillo, M. Gerhardt, and P. Aichroth, “Audio spectrogram transformer for synthetic speech detection via speech formant analysis,” in *IEEE International Workshop on Information Forensics and Security (WIFS)*, Nuremberg, Germany, 2023.
- [10] L. Cuccovillo, M. Gerhardt, and P. Aichroth, “Audio transformer for synthetic speech detection via formant magnitude and phase analysis,” in *IEEE International Conference on Acoustics, Speech and Signal Processing (ICASSP)*, Seoul, South Korea, 2024.
- [11] L. Cuccovillo, M. Gerhardt, and P. Aichroth, “Audio transformer for synthetic speech detection via multi-formant analysis,” in *IEEE/CVF Conference on Computer Vision and Pattern Recognition Workshops (CVPRW)*, Seattle, WA, USA, 2024, pp. 4409–4417.
- [12] H. Tak, J. Patino, M. Todisco, A. Nautsch, N. Evans, and A. Larcher, “End-to-end anti-spoofing with rawnet2,” in *IEEE International Conference on Acoustics, Speech and Signal Processing (ICASSP)*, Toronto, ON, Canada, 2021, pp. 6369–6373.
- [13] J.-w. Jung et al., “AASIST: Audio anti-spoofing using integrated spectro-temporal graph attention networks,” in *IEEE International Conference on Acoustics, Speech and Signal Processing (ICASSP)*, Singapore, Singapore, 2022, pp. 6367–6371.
- [14] A. Vaswani et al., “Attention is all you need,” in *International Conference on Neural Information Processing Systems (NeurIPS)*, Long Beach, CA, USA, 2017, pp. 5998–6008.
- [15] J. M. Martín Doñas, A. Álvarez, E. Roselló Casado, Á. M. Gómez García, A. M. Peinado Herreros, et al., “Exploring self-supervised embeddings and synthetic data augmentation for robust audio deepfake detection,” in *ISCA Interspeech*, Incheon, South Korea, 2022.
- [16] Y. Xiao and N. T. Vu, “Layer-wise decision fusion for fake audio detection using XLS-R,” in *ISCA Interspeech*, Rotterdam, The Netherlands, 2025, pp. 5618–5622.
- [17] X. Wang et al., “ASVspoof 5: Design, collection and validation of resources for spoofing, deepfake, and adversarial attack detection using crowdsourced speech,” *Computer Speech & Language*, p. 101 825, 2025.
- [18] N. Müller, P. Czempin, F. Dieckmann, A. Froghyar, and K. Böttiger, “Does audio deepfake detection generalize?” In *ISCA Interspeech*, Incheon, South Korea, 2022, pp. 2783–2787.
- [19] R. Reimao and V. Tzerpos, “FoR: A dataset for synthetic speech detection,” in *IEEE International Conference on Speech Technology and Human-Computer Dialogue (SpeD)*, Timisoara, Romania, 2019, pp. 1–10.
- [20] D. Salvi, B. Hosler, P. Bestagini, M. C. Stamm, and S. Tubaro, “TIMIT-TTS: a text-to-speech dataset for multimodal synthetic media detection,” *IEEE Access*, vol. 11, pp. 50 851–50 866, 2023.
- [21] C. Sanderson, “The VidTIMIT database,” IDIAP Research Institute, Tech. Rep., 2002. [Online]. Available: <https://doi.org/10.5281/zenodo.158963>
- [22] M. Mauch and S. Dixon, “pYIN: A fundamental frequency estimator using probabilistic threshold distributions,” in *IEEE International Conference on Acoustics, Speech and Signal Processing (ICASSP)*, Florence, Italy, 2014, pp. 659–663.
- [23] Y. Jadoul, B. Thompson, and B. de Boer, “Introducing Parselmouth: A Python interface to Praat,” *Journal of Phonetics*, vol. 71, pp. 1–15, 2018.
- [24] P. Boersma and D. Weenink, *Praat: Doing phonetics by computer [Computer program]*, Version 6.1.38, retrieved 2 January 2021 <http://www.praat.org/>, 2021.